Scientific Assessment, J. T. Houghton *et al.*, Eds. (Cambridge Univ. Press, Cambridge, 1990).
3. R. Wetherald, S. Manabe, *J. Atmos. Sci.* **45**, 1397 (1988).
4. R. Cess *et al.*, *J. Geophys. Res.* **95**, 16601 (1989).
5. I. Held, B. Soden, *Annu. Rev. Energy Environ.* **25**, 441, (2000).
6. R. Lindzen, *Bull. Am. Meteorol. Soc.* **71**, 288 (1990).
7. R. E. Dickinson *et al.*, in *Climate Change 1995: The Science of Climate Change*, J. T. Houghton *et al.*, Eds. (Cambridge Univ. Press, Cambridge, 1996).
8. A. Raval, V. Ramathan, *Nature* **342**, 758 (1989).
9. F. Wentz, M. Schabel, *Nature* **403**, 414 (2000).
10. D. Rind *et al.*, *Nature* **349**, 500 (1991).
11. A. Del Genio, W. Kovari, Y. Mao-Sung, *Geophys. Res. Lett.* **21**, 2701 (1994).
12. B. Soden, *J. Clim.* **10**, 1050 (1997).
13. S. Bony, J. Duvel, H. Le Treut, *Clim. Dyn.* **11**, 307 (1995).
14. K. Lau, C. Ho, M. Chou, *Geophys Res. Lett.* **23**, 2971 (1996).
15. A. Inamdar, V. Ramanthan, *J. Geophys. Res.* **103**, 32177 (1998).
16. B. Franklin, *Manchester Literary and Philosophical Society Memoirs and Proceedings*, **2**, 122 (1784) [Reprinted in *Weatherwise*, **35**, 262 (1982)].
17. A. Robock, *Rev. Geophys.* **38**, 191 (2000).
18. J. Hansen, A. Lacis, R. Ruedy, M. Sato, *Geophys. Res. Lett.* **19**, 215 (1992).
19. I. Kirchner *et al.*, *J. Geophys. Res.* **104**, 19039 (1999).
20. L. Stowe, R. Carey, P. Pellegrino, *Geophys. Res. Lett.* **19**, 159 (1992).
21. C. Trepte, R. Veiga, M. McCormick, *J. Geophys. Res.* **98**, 18563 (1993).
22. P. Minnis *et al.*, *Science* **259**, 1411 (1993).
23. A. Robock, J. Mao, *J. Clim.* **8**, 1086 (1992).
24. D. Parker, H. Wilson, J. Christy, C. Folland, *Int. J. Clim.* **16**, 487 (1996).
25. D. Randel *et al.*, *Bull. Am. Meteorol. Soc.* **77**, 1233 (1996).
26. Supplemental material is available at *Science* Online at www.sciencemag.org/cgi/content/full/296/5568/727/DC1.
27. A. Hall, S. Manabe, *J. Clim.* **12**, 2327 (1999).
28. The atmospheric model is a global spectral model with rhomboidal truncation at 30 wave numbers and 14 vertical levels. Details regarding the model's numerical formulation and physical parameterizations may be found in (*26*). The thickness of the ocean mixed-layer varies regionally and is specified according to its observed annual-mean climatology (S. Levitus, *NOAA Prof. Paper* 13, 1982).
29. G. Stenchikov *et al.*, *J. Geophys. Res.* **103**, 13837 (1998).
30. Beginning in 1994, additional anomalies in the satellite-observations of top-of-atmosphere absorbed solar radiation become evident, which are unrelated to the Mount Pinatubo eruption and therefore not reproduced in the model simulations. These anomalies are believed to stem from decadal-scale changes in the tropical circulation over the mid- to late 1990's [see J. Chen *et al.*, *Science* **295**, 838 (2002); and B. A. Wielicki *et al.*, *Science* **295**, 841 (2002)], but their veracity remains the subject of debate. If real, their absence in the model simulations implies that discrepancies between the observed and model-simulated temperature anomalies, delayed ~ 1 to 2 years by the climate system's thermal inertia, may occur by the mid-1990s. We therefore limit our analysis to the 5-year period 1991–1995, where the observations and model simulations are responding to similar changes in radiative forcing and encompass virtually all of the observed climate response to Pinatubo.
31. J. Christy, R. Spencer, W. Braswell, *J. Atmos. Oceanic Tech.* **17**, 1153 (2000).
32. A static, global weighting function is used to compute the equivalent lower tropospheric temperatures (2LT) from the model-simulated temperature profiles. See (*44*).
33. B. Santer *et al.*, *J. Geophys. Res.* **106**, 28033 (2001).
34. P. Udelhofen, D. Hartmann, *J. Geophys. Res.* **100**, 7423 (1995).
35. J. Susskind *et al.*, *Bull. Am. Meteorol. Soc.* **78**, 1449 (1997).
36. C. Rodgers, *Rev. Geophys. Space Phys.* **14**, 609 (1976).
37. We use intercalibrated, cloud-cleared radiances from the TOVS Radiance Pathfinder Project (*45*).
38. The "GCM-predicted" $T_{6.7}$ was computed offline by inserting the GCM profiles of temperature, water vapor mixing ratio, and Mount Pinatubo aerosols into a narrow band radiative transfer model (*46*). These results were then subtracted from the $T_{6.7}$ computed using the control simulations of temperature and water vapor mixing ratio, and the difference was plotted in Fig. 3.
39. Because, the $T_{6.7}$ depends on both Planck emission (temperature) and atmospheric opacity (water vapor mass), variations in $T_{6.7}$ cannot be unambiguously related to changes in water vapor mass, but rather are largely determined by changes in relative humidity (*47*, *48*).
40. The "constant rh" $T_{6.7}$ was calculated as in (*38*), but replacing the model-predicted water vapor mixing ratio with that obtained by fixing the relative humidity to its seasonally varying climatological value. Thus as the atmosphere cools, the mixing ratio used to compute the $T_{6.7}$ decreases at a constant relative humidity rate.
41. The "no drying" $T_{6.7}$ was calculated as in (*38*), but replacing the model-predicted water vapor mixing ratio with its seasonally varying climatological value. Thus, as the atmosphere cools, the mixing ratio used to compute the $T_{6.7}$ remains unchanged.
42. We follow the same procedure as Hall and Manabe (*27*) in configuring the "no water vapor feedback" version of the GCM.
43. Santer *et al.* (*33*) provide three different estimates of the MSU lower tropospheric temperature (2LT) record, which differ according to the index used to remove the ENSO signal. The time-average, global-mean cooling for the three versions of their data are 0.29 K (Niño 3 index). 0.32 K (Niño 3.4 index), and 0.36 K (SOI index). Because our results are insensitive to which version is used, for clarity, we have plotted only the intermediate of the three versions (Niño 3,4 index) in Figs. 2 and 4.
44. B. Santer *et al.*, *J. Geophys. Res.* **104**, 6305 (1999).
45. J. Bates, X. Wu, D. Jackson, *J. Clim.* **9**, 427 (1996).
46. B. Soden *et al.*, *Bull. Am. Meteorol. Soc.* **81**, 797 (2000).
47. F. Moller, *Planet. Space Sci.* **5**, 202 (1963).
48. B. Soden, F. Bretherton, *J. Geophys. Res.* **98**, 16669 (1993).

49. We acknowledge contributions and assistance from I. Held, V. Ramaswamy, N. C. Lau, A. Hall, J. Bates, D. Randel, B. Santer, J. Susskind, and T. Von der Haar; and we thank S. Solomon for early discussions and encouragement that eventually led to this study. Partially supported by NASA grant NAG 5-9792, NSF grant ATM-9988419.

7 February 2002; accepted 19 March 2002

The North Atlantic Spring Phytoplankton Bloom and Sverdrup's Critical Depth Hypothesis

D. A. Siegel,[1]* S. C. Doney,[2] J. A. Yoder[3]

More than 50 years ago, Harald Sverdrup developed a simple model for the necessary conditions leading to the spring bloom of phytoplankton. Although this model has been used extensively across a variety of aquatic ecosystems, its application requires knowledge of community compensation irradiance (I_C), the light level where photosynthetic and ecosystem community loss processes balance. However, reported I_C values have varied by an order of magnitude. Here, I_C estimates are determined using satellite and hydrographic data sets consistent with the assumptions in Sverdrup's 1953 critical depth hypothesis. Retrieved values of I_C are approximately uniform throughout much of the North Atlantic with a mean value of 1.3 mol photons meter^{-2} day^{-1}. These community-based I_C determinations are roughly twice typical values found for phytoplankton alone indicating that phytoplankton account for approximately one-half of community ecosystem losses. This work also suggests that important aspects of heterotrophic community dynamics can be assessed using satellite observations.

The spring bloom of phytoplankton in the North Atlantic Ocean has long fascinated oceanographers from the 1930s to 1950s (*1*–*3*) to the present day, where large interdisciplinary field experiments have been conducted to assess its role in the global carbon cycle (*4*). When viewed from space, the North Atlantic spring bloom is among the largest mass greenings observed on the Earth surface extending over scales of more than 2000 km (*5*–*7*). The North Atlantic spring bloom propagates to the north at speeds of the order of 20 km day^{-1} as can be clearly seen in time series observations of chlorophyll pigment concentration (Chl) made from spaceborne sensors (*8*).

Sverdrup's 1953 critical depth hypothesis (*1*) has been applied to a variety of aquatic ecosystems in an effort to quantify the roles of light availability and vertical mixing leading to spring blooms of phyto-

[1]Institute for Computational Earth System Science and Department of Geography, University of California Santa Barbara, Santa Barbara, CA 93106–3060, USA. [2]National Center for Atmospheric Research, 1850 Table Mesa Drive, Boulder, CO 80305, USA. [3]Graduate School of Oceanography, University of Rhode Island, Narragansett, RI 02882–1197, USA.

*To whom correspondence should be addressed. E-mail: davey@icess.ucsb.edu

plankton (*9–13*). This simple model assumes that under nutrient replete conditions primary production, $P(z)$, is linearly related to the light flux, $I(z)$, and that the effects of community respiration and other loss processes, $R(z)$, are depth independent, or

$$P(z) = \alpha I(z) = \alpha I_o e^{-Kz} = P_o e^{-Kz} \quad (1a)$$

$$R(z) = R_o \quad (1b)$$

where α is the slope of the light-productivity relationship, I_o is the flux of incident photosynthetically available radiation (PAR), K is the diffuse attenuation coefficient for PAR, P_o is the surface productivity ($= \alpha I_o$), and z is depth within the water column. Community loss processes include autotrophic and heterotrophic respiration, grazing, excretion, and vertical export by sinking particles (*10, 14*). Net production occurs above depths where $P(z)$ is greater than R_o and the depth where these rates are equal defines the compensation depth, Z_C [$= (1/K) \ln(P_o/R_o)$] or alternatively the compensation irradiance, I_C ($= I_o R_o / P_o$).

Net community production, and thereby the initiation of a spring bloom, occurs when the vertically integrated net productivity is greater than the integrated loss rates. Sverdrup's critical depth, Z_{CR}, is defined as the depth where these integrated rates are equal. If the depth of the ocean mixed layer, Z_{ML}, is greater than Z_{CR}, there is insufficient light to drive net production and rapid increases in phytoplankton biomass will not occur. Spring shoaling of the mixed layer to depths less than Z_{CR} elevates the average light of the mixed layer, increasing mixed layer average rates of production. This increase of production over community losses initiates the spring bloom and leads to rapid increases in phytoplankton standing stocks. Values for Z_{CR} can be derived if estimates of I_o, K, and I_C are available following

$$\frac{1}{KZ_{CR}}\left(1 - e^{-KZ_{CR}}\right) = \frac{R_0}{P_0} = \frac{I_C}{I_0} \quad (2)$$

Key to the application of Sverdrup's critical depth hypothesis is knowledge of the compensation irradiance as the other terms are relatively easy to constrain. Values of I_C often come from phytoplankton culture experiments assessing the minimum irradiance required for a population to survive. Sverdrup assumed a value for I_C of ~0.6 mol photons m^{-2} day^{-1}, on the basis of previous phytoplankton culture studies (*1*), and this exact value is still in use (*12*). A compilation of recent laboratory-derived compensation irradiance determinations over a range of phytoplankton species gives values of I_C ranging from 0.1 to 0.8 mol photons m^{-2} day^{-1} (*15*). However, these phytoplankton-based I_C estimates do not account for many of the loss processes in pelagic communities and are likely to be lower bounds for the true community I_C values (*1, 10, 14*). Observations by Riley in 1957 (*3*) suggest a community-level I_C of 3.5 mol photons m^{-2} day^{-1} (*16*), and this value has been used by several investigators (*11, 17*). However, a recent analysis of seasonal dissolved oxygen cycles found a North Atlantic mean, community-level I_C of 1 W m^{-2} (~0.35 mol photons m^{-2} day^{-1}), which is nearly one-half of typical phytoplankton I_C values (*18*). All told, reported I_C values range over a full order of magnitude, from 0.35 to 3.5 mol photons m^{-2} day^{-1}. Our goal is to provide consistent community-level estimates of I_C by assessing the time/space characteristics of the North Atlantic spring bloom. This results in a partitioning between the autotrophic and heterotrophic ecosystem components during the initiation of the spring bloom. The approach can also provide quantitative determinations of community loss processes, which remain poorly characterized compared to ocean primary production rates (*19*).

Satellite ocean color imagery from the Sea-viewing Wide Field-of-view Sensor (SeaWiFS) mission are used to assess chlorophyll and incident PAR flux distributions for the North Atlantic Ocean (*20*). The timing of a spring bloom can be diagnosed by evaluating the year/day where events in a Chl time record occur. For example, the day when the maximum Chl concentration occurs, YD_{MaxChl}, provides one useful index. However, YD_{MaxChl} occurs during the peak of the bloom (Table 1), and it will not be useful for diagnosing spring bloom initiation (*7*). The year/day where Chl levels first rise a small threshold above median values is found to be a reasonable index for bloom initiation, because a bloom should correspond to a large

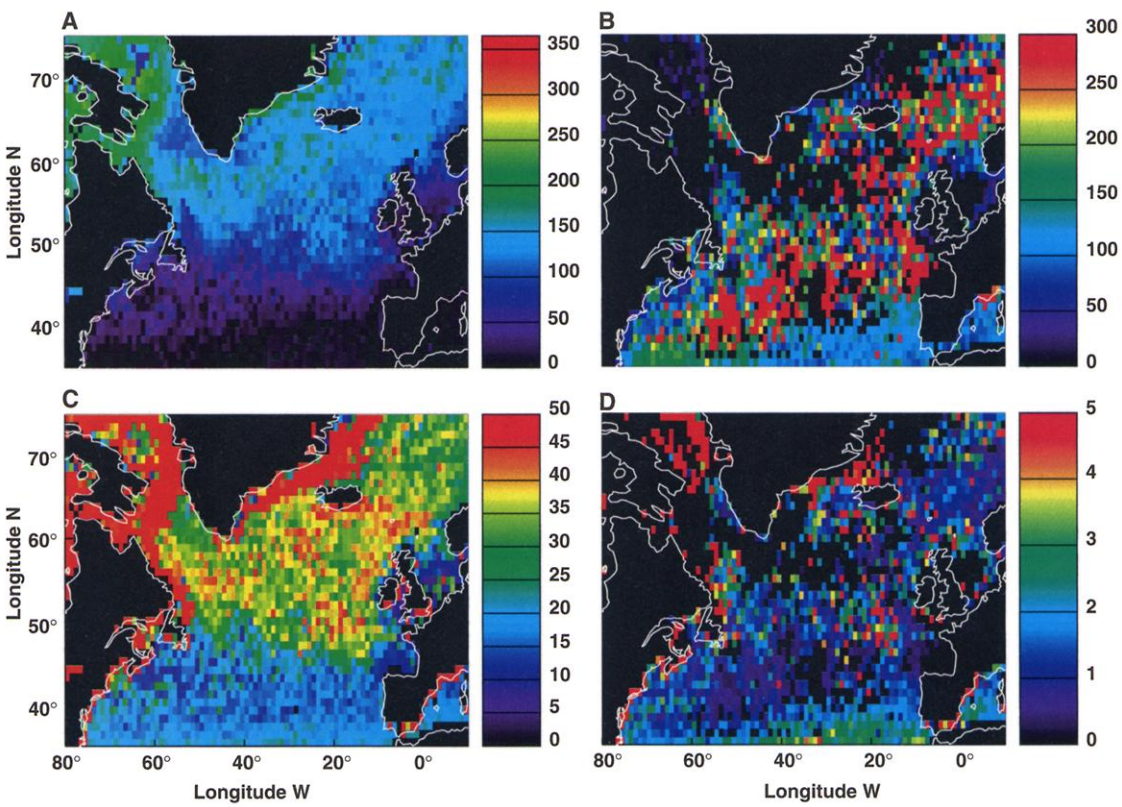

Fig. 1. Spatial distributions of (**A**) year/day of bloom initiation (YD_{init}; Julian day of the year starting with January 1), (**B**) mixed layer depth at YD_{init} (Z_{MLD} in meters), (**C**) incident photosynthetically available radiation at YD_{init} (I_o in mol photons m^{-2} day^{-1}), and (**D**) community compensation irradiance (I_C in mol photons m^{-2} day^{-1}). Climatological values of Z_{MLD} and I_C are plotted only if more than five independent observations went into the Z_{MLD} climatology (*22*). SeaWiFS data for years 1998, 1999, and 2000 are averaged together to provide an appropriate climatology.

increase in biomass above normal (i.e., median) conditions (*21*). Little quantitative differences in the resulting computations were found using thresholds ranging from 1 to 30%, and a final value of 5% was selected (hereafter denoted YD_{init}).

The spatial distribution of YD_{init} shows the expected northward propagation of the spring bloom (Fig. 1A). South of 40°N, the bloom starts early in the year (YD 32 is February 1), whereas north of 50°N, the bloom start is much later (YD 152 is June 1). Two distinct zones of spring bloom initiation are apparent. From 35°N to 50°N, the year/day for bloom initiation increases steadily (from YD 13 to 112), whereas north of about 50°N, YD_{init} increases only marginally over a scale of ~2000 km (Fig. 1A and Table 1). Superimposed on these latitudinal trends in YD_{init} values are large-scale features that appear related to seasonal ice zone processes and topographic features.

Following Sverdrup's hypothesis, the depth of the mixed layer, Z_{MLD}, at the time of bloom initiation defines the critical depth, Z_{CR}. Monthly mean mixed layer depth estimates are taken from available oceanographic climatologies (*22*) and are interpolated to YD_{init} (Fig. 1B). Values of Z_{MLD} during bloom initiation show no obvious latitudinal trends for latitudes greater than 40°N (Table 1). Deep mixed layer depths are found in the subtropical gyre due to the convergence of Ekman surface water transports (*23, 24*). A large degree of variability about these general trends is observed, which is due to the relatively few data points contributing to the Z_{MLD} climatology (*22*).

The incident PAR flux (*25*) at bloom initiation shows a counterintuitive pattern where I_o actually increases to the north (Fig. 1C). This is due simply to increased day length as the spring bloom progresses northward. Values of I_o are more than twofold lower between 35°N and 40°N than they are north of 55°N (Table 1).

Climatological fields for I_C can now be determined using the data sets presented and estimates of the depth penetration for PAR (*26*). Although many outliers exist, values of I_C are roughly uniform north of 40°N with typical values between 1 and 1.5 mol photons m^{-2} day^{-1} (Fig. 1D). Median I_C retrievals for 5° bands of latitude are equal to 1.3 (± 0.3 SD) mol photons m^{-2} day^{-1} north of 40°N (Table 1). Interestingly, these I_C estimates are seemingly constant over six or more distinct biogeochemical provinces (*21*). Values for the compensation depth, Z_C, show a decrease with latitude starting at 31 m at 35°N and rising to about 22 m north of 50°N (Table 1). Thus, Z_C lies far above the 1% PAR isolume. The present determinations of I_C are roughly two times larger than typical values for phytoplankton respiration alone, suggesting that phytoplankton processes contribute about one-half of the total community losses of fixed carbon. South of 40°N, median values of I_C increase significantly (Table 1). These changes are particularly apparent in the eastern portion of the basin where shallow mixed layers increase retrieved values of I_C to ~3 mol photons m^{-2} day^{-1} (Fig. 1D).

The retrieved I_C distributions suggest that there are two distinct regimes for spring bloom dynamics in the North Atlantic Ocean (Fig. 1D and Table 1) (*27*). North of ~40°N, deep winter mixing elevates surface water nutrient concentrations; however, this mixing also reduces the average irradiance within the mixed layer to below community compensation. Once the mixed layer depth shallows, a spring bloom occurs following Sverdrup's 1953 hypothesis. South of 40°N especially in the eastern basin, winter mixing is less vigorous and the ecosystem is likely to be limited by nutrients rather than by light. Hence, the spring bloom is initiated by the supply of nutrients from winter mixing, and the conditions required by Sverdrup's 1953 hypothesis do not hold (*27*). Differences in nutrient supply may also create changes in plankton community structure between the two domains (*28*).

The present results suggest a role of prebloom community structure on the timing of the North Atlantic spring bloom [see also (*7*)]. Prior to the spring bloom, autotrophic production balances community losses, and these losses appear to be partitioned equally between autotrophic respiration and the sum of heterotrophic respiration, grazing, and export processes. When physical factors enable phytoplankton production to exceed community losses, the balance breaks down and a bloom can occur. The structure of the prebloom heterotrophic community is therefore important to the initiation of the bloom. If the grazers in the community are able to increase their biomass fast enough to keep pace with the blooming autotrophs, then a bloom may be arrested. If not, a bloom can proceed unimpeded.

The present estimates of community compensation provide a potentially powerful way of quantifying heterotrophic processes from satellite data sets. Used along with appropriate measures of autotrophic biomass and productivity, interannual variations of heterotrophic rate processes can be assessed. In particular, this approach may be a great tool for understanding the consequences of the North Atlantic Oscillation on ecosystem function and structure (*29, 30*). Clearly, improvements must be made to presently available estimates of mixed layer properties and spring bloom characteristics. It seems likely that numerical modeling and data assimilation approaches will mature rapidly, enabling these interannual changes to be appropriately assessed (*31, 32*). Once this is achieved, consistent analyses of organic carbon energy flow by heterotrophs and autotrophs could be made using satellite-borne data systems.

Table 1. Zonal statistics characterizing the North Atlantic spring bloom. Median values of each quantity are estimated for each zonal band of latitudes. Median statistics are used to eliminate the influence of rare large outliers. Observations from coastal regions and inland or marginal seas are not included. In addition, individual estimates are included in the zonal statistics only if more than five independent observations of mixed layer depth are used in constructing the monthly mixed layer depth climatology for each 1° by 1° box.

Zone (°N)	YD_{init} (day)	YD_{MaxChl} (day)	Z_{MLD} (m)	$Z_{1\%PAR}$ (m)	$\frac{Z_{MLD}}{Z_{1\%PAR}}$	I_C/I_O (%)	$\left(\frac{I_O}{\text{mol photon}/m^2\ d}\right)$	$\left(\frac{I_C}{\text{mol photon}/m^2\ d}\right)$	Z_C (m)	$\frac{Z_C}{Z_{1\%PAR}}$
35–40	13	99	127	63	2.1	10.2	17.5	1.69	31	0.50
40–45	33	117	181	49	3.9	5.5	17.8	0.96	31	0.63
45–50	82	143	205	40	5.2	4.2	28.3	1.24	28	0.69
50–55	112	163	146	35	4.5	4.9	35.2	1.63	23	0.65
55–60	129	173	147	34	4.3	5.1	34.3	1.75	22	0.65
60–65	134	178	185	33	5.8	3.7	39.9	1.33	24	0.72
65–70	137	173	22	333	6.6	3.3	37.4	1.02	24	0.74
70–75	143	172	192	32	5.4	4.0	36.2	1.37	22	0.70

References and Notes

1. H. U. Sverdrup, *J. Cons. Perm. Int. Explor. Mer.* **18**, 287 (1953).
2. H. H. Gran, *Rapp. Proc. Verb. Cons. Int. Explor. Mer.* **75**, 37 (1931).
3. G. A. Riley, *Limnol. Oceanogr.* **2**, 252 (1957).
4. H. W. Ducklow, R. Harris, *Deep-Sea Res. II* **40**, 1 (1993).
5. C. R. McClain *et al.*, *J. Geophys. Res.* **95**, 18027 (1990).
6. J. A. Yoder, C. R. McClain, G. C. Feldman, W. E. Esaias, *Global Biogeochem. Cycles* **7**, 181 (1993).
7. K. Banse, D. C. English, *J. Geophys. Res.* **99**, 7323 (1994).
8. See http://daac.gsfc.nasa.gov/CAMPAIGN_DOCS/OCDST/nab.html (or www.icess.ucsb.edu/~davey/NorthAtlanticBloom.htm).
9. D. M. Nelson, W. O. Smith, *Limnol. Oceanogr.* **36**, 1650 (1991).
10. T. Platt, D. F. Bird, S. Sathyendranath, *Proc. R. Soc. London Ser. B* **245**, 205 (1991).
11. D. W. Townsend, M. D. Keller, M. E. Sieracki, S. G. Ackleson, *Nature* **260**, 59 (1992).
12. A. Obata, J. Ishizaka, M. Endoh, *J. Geophys. Res.* **101**, 20657 (1996).
13. L. V. Lucas, J. E. Cloern, J. R. Koseff, S. G. Monismith, J. K. Thompson, *J. Mar. Res.* **56**, 375 (1998).
14. V. Smetacek, U. Passow, *Limnol. Oceanogr.* **35**, 228 (1990).
15. C. Langdon, *J. Plankton Res.* **10**, 1291 (1988). Note: Two relatively high I_C determinations for coastal dinoflagellate species were removed from the range presented in the text as these are not likely to be relevant for the North Atlantic Ocean.
16. Riley's original value in 1957 (*3*) of 0.3 g-cal cm^{-2} min^{-1} for critical irradiance for net production is converted into estimates of I_C in quanta units by applying Eqs. 1 through 3 and assuming that 50% of

the total solar flux is in the PAR band and that 1 joule = 2.5×10^{18} photons in the PAR band.
17. W. W. C. Gieskes, G. W. Kraay, *Neth. J. Sea Res.* **9**, 166 (1975).
18. We believe that the inconsistency between the O_2-derived estimates of I_C and those presented here (and elsewhere) is due to fundamental differences between the processes regulating annual O_2 cycles and those responsible for initiating spring phytoplankton blooms. R. G. Najjar and R. F. Keeling [*J. Mar. Res.* **55**, 117 (1997)] related the depth where the vertical O_2 profile switches sign from net production to net consumption as the compensation depth, by using a harmonic analysis over the annual cycle. This "nodal depth" is influenced by a variety of processes not directly relevant to the initiation of a spring bloom including diapycnal mixing, degassing, and particle sinking and remineralization. The harmonic analysis uses O_2 observations from throughout the annual cycle, not all of which are relevant for spring blooms. Last, typical values of the photosynthetic quota (carbon assimilated by phytoplankton per O_2 evolved) will be smaller for phytoplankton grown on ammonia (recycling communities) than those grown on nitrate (bloom communities). This should result in a 20% or so underestimate in the I_C value estimated using the seasonal O_2 cycle. In short, we believe for a number of reasons that analyses of the seasonal O_2 profile will not provide I_C estimates appropriate for diagnosing the initiation of a spring bloom. Clearly, resolution of this issue is beyond the scope of the present contribution, and it is likely that this issue is best resolved via a detailed modeling evaluation.
19. M. J. Behrenfeld *et al.*, *Science* **291**, 2594 (2001).
20. C.R. McClain *et al.*, *Sea Technol.* **39**, 10 (1988). Note: Level 3, global area coverage (GAC; 9 km resolution) SeaWiFS determinations of chlorophyll pigment concentration are used for determining the onset of the spring bloom and its properties. For calculations performed, 8-day composite SeaWiFS chlorophyll fields are aggregated to a 1° by 1° spatial resolution. Calculations are done for years 1998, 1999, and 2000 separately and then averaged together to provide a climatological estimate for the North Atlantic Spring bloom.
21. A. R. Longhurst, *Ecological Geography of the Sea* (Academic Press, San Diego, CA, 1988).
22. Climatological estimates of monthly mean mixed layer depth are derived using data from the World Ocean Atlas 98 [J. Antonov *et al.*, *World Ocean Atlas 1998*, vol. 1, *Temperature of the Atlantic Ocean*, NOAA Atlas NESDIS 27. (US Government Printing Office, Washington, DC, 1998)] assuming a 0.5°C temperature difference from the sea surface temperature [G. Monterey, S. Levitus, *Seasonal Variability of Mixed Layer Depth for the World Ocean*. NOAA Atlas NESDIS 14 (US Government Printing Office, Washington, DC, 1997)]. Mixed layer depth estimates as well as the number of observations going into those monthly climatological mean values are available from http://las.pfeg.noaa.gov/las/ on a 1° by 1° basis. Estimates of Z_{MLD} are used only if there are more than five independent observations monthly for each 1° by 1° subregion.
23. C. R. McClain, J. K. Firestone, *J. Geophys. Res.* **98**, 12327 (1993).
24. R. G. Williams, M. J. Follows, *Deep-Sea Res. I* **45**, 461 (1998).
25. Incident PAR imagery are averaged over the same 8-day period and grid as the SeaWiFS chlorophyll product. Documentation for the SeaWiFS PAR product is available at http://orca.gsfc.nasa.gov/seawifs/par/doc/seawifs_par_wfigs.pdf. Units are mol photons m^{-2} day^{-1}.
26. The depth penetration of PAR is calculated using $Z_{1\%PAR} = 38.0\ Chl_{BL}^{-0.428}$, where $Z_{1\%PAR}$ is the 1% PAR isolume depth and Chl_{BL} is the surface chlorophyll concentration (mg m^{-3}) as the spring bloom starts. Note that $Z_{1\%PAR} = 4.6/K$ where K is the diffuse attenuation coefficient [A. Morel, *J. Geophys. Res.* **93**, 10749 (1988)].
27. S. Dutkiewicz, M. Follows, J. Marshall, W. W. Gregg, *Deep-Sea Res. II* **48**, 2323 (2001).
28. D. A. Siegel *et al.*, *J. Mar. Res.* **48**, 379 (1990).
29. J.-M. Fromentin, B. Planque, *Mar. Ecol.-Prog. Ser.* **134**, 111 (1996).
30. R. G. Williams, A. J. McLaren, M. J. Follows, *Global Biogeochem. Cycles* **14**, 1299 (2000).
31. S. C. Doney, *Global Biogeochem. Cycles* **13**, 705 (1999).
32. J. A. Carton, G. Chepurin, X. Cao, B. S. Giese, *J. Phys. Oceanogr.* **30**, 294 (2000).
33. We thank M. Lorenzi-Kayser for computational assistance and M. Abbott, C. Carlson, H. Ducklow, and A. Michaels for comments and discussion. This work is supported by NASA and NSF.

19 December 2001; accepted 19 March 2002

Role of Yersinia Murine Toxin in Survival of *Yersinia pestis* in the Midgut of the Flea Vector

B. Joseph Hinnebusch,[1]* Amy E. Rudolph,[2]† Peter Cherepanov,[3] Jack E. Dixon,[2] Tom G. Schwan,[1] Åke Forsberg[3]

Transmission by flea bite is a relatively recent adaptation that distinguishes *Yersinia pestis*, the plague bacillus, from closely related enteric bacteria. Here, a plasmid-encoded phospholipase D (PLD), previously characterized as Yersinia murine toxin (Ymt), was shown to be required for survival of *Y. pestis* in the midgut of its principal vector, the rat flea *Xenopsylla cheopis*. Intracellular PLD activity appeared to protect *Y. pestis* from a cytotoxic digestion product of blood plasma in the flea gut. By enabling colonization of the flea midgut, acquisition of this PLD may have precipitated the transition of *Y. pestis* to obligate arthropod-borne transmission.

Y. pestis, the highly virulent flea-borne agent of bubonic plague, is a recently emerged clone of *Yersinia pseudotuberculosis*, which causes a relatively mild food- and water-borne enteric disease (*1*). A major genetic difference between them is the presence of two *Y. pestis*–specific plasmids, one of which contains the gene for Ymt (*2–5*), a phospholipase D (PLD) (*6*). Murine toxin was characterized as a protein fraction of *Y. pestis* in the 1950s (*7*) and later shown to have β-adrenergic blocking ability (*8*). Toxicity is manifested by hypotension and vascular collapse when Ymt is released from lysing bacteria at the terminal stage of septicemic plague (*9*, *10*). *Y. pestis* Ymt has since been shown to belong to a family of PLD enzymes, characterized by conserved HKD ($HXKX_4DX_6GG/S$; X, any amino acid) catalytic motifs, found in plants, animals, fungi, bacteria, and eukaryotic viruses (*6*, *11–13*). Because Ymt is toxic to mice and rats but not to other animals (*9*, *10*), it has been presumed that the high lethality of plague for mice is partly attributable to Ymt. However, the lethal dose of *Y. pestis* in mouse infection models is not changed significantly by deletion of *ymt* (*14–16*). This, and the fact that *ymt* expression is greater at 26°C than at 37°C (*15*), prompted us to investigate a role for Ymt in the insect vector. We infected *X. cheopis* fleas with Ymt^+ or isogenic Ymt^- *Y. pestis* and monitored them for 4 weeks after the infectious blood meal (*17*). To produce a transmissible infection, wild-type *Y. pestis* multiplies in the flea midgut to form cohesive aggregates. In some fleas, bacteria eventually fill the proventriculus (a valve that connects the esophagus to the midgut) and block normal blood feeding. Blocked fleas transmit plague efficiently because during their persistent efforts to feed, plague bacilli are dislodged from the proventriculus into the bite site (*18*). *Y. pestis ymt*H188N, a strain that synthesizes a mutant form of Ymt in which a single amino acid change in one of the two HKD catalytic motifs reduces PLD activity by >99% (*6*), did not block any of 319 fleas examined (Table 1). In contrast, the isogenic parent *Y. pestis* KIM6+ blocked 24 to 38% of fleas and caused high mortality due to blockage-induced starvation. Complementation of the *ymt*H188N mutant by transformation with pCH16, a plasmid that contained a wild-type copy of *ymt*, restored the normal blockage rate. Similarly, a *ymt* deletion mutant of *Y. pestis* that blocked only 3 of 310 fleas regained normal blockage capability when complemented with *ymt*.

Because blockage depends on prior colonization of the digestive tract, we assessed the infection rate and bacterial load of fleas at various times after a single infectious blood meal (*17*) (Fig. 1). *Y. pestis* KIM6+ established chronic infection in 50 to 80% of fleas, the normal infection rate (*19*, *20*), but the *ymt*H188N mutant was eliminated from 80 to 95% of fleas within the first 24 hours, and the average number of viable bacteria per positive flea decreased from 4.7×10^4 to 250 during the first 24 hours. Similar results were obtained from fleas infected with the *Y. pestis ymt* dele-

[1]Laboratory of Human Bacterial Pathogenesis, Rocky Mountain Laboratories, National Institute of Allergy and Infectious Diseases, National Institutes of Health, Hamilton, MT 59840, USA. [2]Department of Biological Chemistry, University of Michigan Medical School, Ann Arbor, MI 48109, USA. [3]Department of Medical Countermeasures, Swedish Defense Research Agency, S-901 82 Umeå, and Department of Molecular Biology, Umeå University, S-901 87 Umeå, Sweden.

*To whom correspondence should be addressed. E-mail: jhinnebusch@niaid.nih.gov

†Present address: Pharmacia Corporation, St. Louis, MO 63167, USA.